DOI: 10.22661/AAPPSBL.2019.29.5.19

Neutron Halo - Recent Experimental Progress at RIBF

TAKASHI NAKAMURA
DEPARTMENT OF PHYSICS, TOKYO INSTITUTE OF TECHNOLOGY

ABSTRACT

A neutron halo in light neutron-rich nuclei along the neutron drip line has characteristic features due to its low-density neutron distribution extending beyond the normal nuclear size. The advent of the new-generation rare isotope beam facility, RIBF at RIKEN, has allowed neutron-halo nuclei in new regions of the nuclear chart to be explored. For nuclei in the island-of-inversion region (neutron-rich Ne, Na, Mg isotopes with the neutron number N∼20) in the nuclear chart, where the conventional magic number N=20 does not persist, breakup reaction experiments on ^{29,31}Ne and ^{37}Mg have shown that these have a new type of halo structure, called a deformation driven p-wave halo. For lighter two-neutron halo nuclei, dineutron correlations corresponding to a spatially-compact neutron pair, have been investigated by quasi-free scattering (scattering of a nucleon inside the nucleus by a relativistic proton) and Coulomb breakup (breakup of a beam particle induced by a pulsed Coulomb field when it passes by a heavy target with relativistic velocity). Recent progress in the experimental research of neutron halo at RIBF is reviewed and discussed.

INTRODUCTION

A neutron halo is extended neutron matter involving one or two valence neutrons surrounding a core with saturated nuclear density, as illustrated for the most traditional halo nucleus ^{11}Li in Fig.1 [1, 2]. In contrast to the common image of an atomic nucleus as being composed of saturated protons and neutrons, a neutron halo has extremely low-density compared to the saturated nuclear density and extends to nearly double the core radius. Before the first operation of RIBF (RI-beam factory) at RIKEN in 2007, the known neutron halo nuclei were limited to ^{6}He, ^{11}Li, ^{11,14}Be,^{17,19}B, and ^{15,19}C. The duality of the core and halo, and the extended neutron distribution lead to the following characteristic reaction properties: 1) large interaction cross section, 2) narrow momentum distribution of the core fragment, and 3) soft E1 excitation (strong electric dipole response at low excitation energies) [3, 4, 5]. Halo nuclei are categorized into 1) two-neutron halo nuclei composed of a core and two halo neutrons, for example, ^{6}He,^{11}Li,^{14}Be,^{17}B, and 2) one-neutron halo nuclei composed of a core and a single-neutron halo, for example, ^{11}Be, and ^{15,19}C. A Halo is formed due primarily to weakly bound neutron(s) with 1n (2n) separation energy S_n (S_{2n}) < ∼1 MeV and quantum tunneling. The other important factor is the low angular momentum, l=0 or 1, of the halo neutron such that it is free from the effect of a centrifugal barrier that would hinder tunneling.

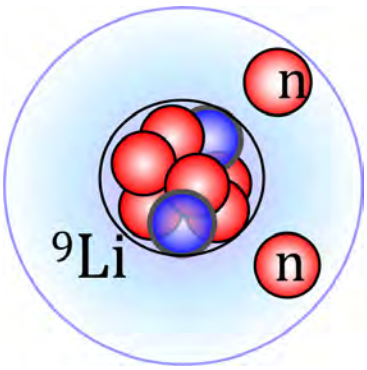

Fig. 1: Schematic view of the two-neutron halo nucleus ^{11}Li that has a dual structure composed of the ^{9}Li core surrounded by a neutron halo involving two neutrons. The radius of the ^{11}Li halo is close to that of ^{208}Pb.

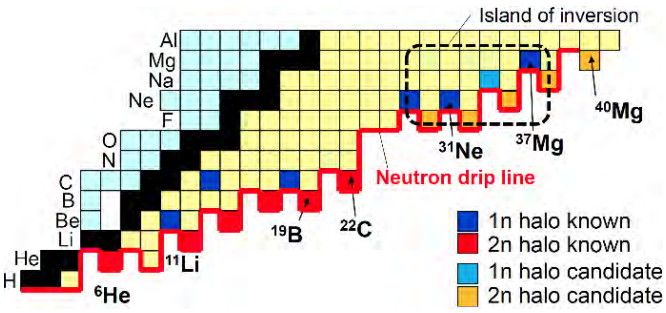

Fig. 2: Halo nuclei, and their candidates are indicated in the nuclear chart. Before the commissioning of RIBF, halo nuclei had been known only up to ^{19}C.

In spite of tremendous experimental and theoretical efforts, it is difficult to predict which nucleus has a halo structure. Indeed, one cannot easily predict the location of halo nuclei in the nuclear chart for heavier nuclei. Even if a halo nucleus is identified, it is still difficult to extract its halo wave function quantitatively. For instance, the interplay between the halo and shell evolution (variation of single-particle levels or shells according to the neutron number and the resultant change of magic numbers) has not been well understood. We need to clarify under what conditions the last neutrons are in an orbital with low angular momentum. Note that some halo nuclei appear where the conventional shell order does not allow a low-l orbital for the valence neutron. We note that shell-gap reduction or shell inversion may happen as in ^{11}Li. Such difficulty can be attributed to the fact that experimentally the neutron drip line has been reached only up to neon isotopes (Z=10, See. Fig.2) [6], and the beam yield of very neutron-rich nuclei near the drip line is very limited [5].

Another interesting question is whether the two neutrons can be more strongly correlated in the halo than in normal nuclei. Migdal has predicted *dineutron* as two spatially-correlated neutrons that behave like a bound pair and appear on the surface of a nucleus [7]. Recently, theoretical efforts have been devoted to this issue in terms of possible dineutron in low-density nuclear matter, such as neutron halo and neutron skin [8, 9]. However, dineutron has not been directly confirmed except for some hints indicated in ^{11}Li [10]. The question of whether multi-neutron halo beyond 2n halo can exist is not clarified yet.

The new-generation RI-beam facility RIBF at RIKEN has offered new opportunities for a wide range of experiments involving halo nuclei. Here, the recent progress in experimental studies of halo nuclei is reported, based on the experiments carried out mainly at RIBF. New halo nuclei, ^{22}C, ^{29,31}Ne, and ^{37}Mg have been confirmed through the experiments at RIBF. In the following sections, after briefly describing the key spectrometers for the experiments on halo nuclei at RIBF, experiments involving new halo nuclei ^{22}C, ^{29,31}Ne, and ^{37}Mg are described. Then I mention briefly the recent experiments on the quasi-free scattering on light halo nuclei.

ZDS and SAMURAI - Key Spectrometers at RIBF

At RIBF, two key spectrometers for exploring the drip line have been constructed: the **Z**ero**D**egree **S**pectrometer (ZDS) [11] and the **S**uperconducting **A**nalyzer for **Mu**lti-particles from **RA**dio Isotope Beam (SAMURAI) [12, 13, 14, 15]. Schematic layouts of ZDS and SAMURAI are shown in Fig.3 and Fig.4, respectively.

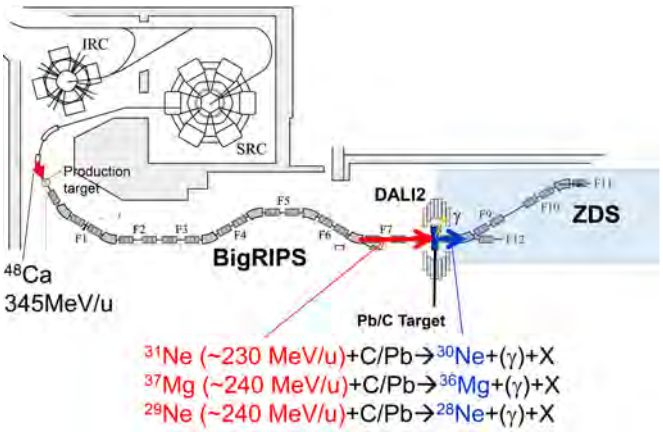

Fig. 3: The layout of ZDS is shown, together with the last two stages of the cyclotron accelerators, IRC, SRC, and the in-flight RI beam separator, BigRIPS at RIBF. As an example, the setup used for the inclusive nuclear and Coulomb breakup of ^{29}Ne [16], ^{31}Ne [17, 18], and ^{37}Mg [19] is schematically shown. BigRIPS is used for separation and particle identification (PID) of the RI beam, while ZDS is used for the PID of the projectile-like fragments.

ZDS, which has been in operation since the beginning of RIBF in 2007, is a two-bend achromatic spectrometer to collect and momentum-analyze the charged particles near the projectile velocity at zero degrees. The momentum resolution P/ΔP is ~1000-6000, depending on the mode [11]. One of the main purposes is an unambiguous particle identification of the projectile-like reaction products with high resolution and medium acceptance. For halo nuclei, ZDS offers a powerful spectroscopic tool for investigating reaction cross sections, and 1n-removal reactions, as such a measurement requires primarily particle identification of incoming and outgoing charged particles. In the latter experiment, one can also obtain the momentum distribution of the projectile-like frag-

ments. As an instance, the setup for the 1n removal of ^{29,31}Ne and ^{37}Mg is shown schematically in Fig. 3. In this case, the de-excitation γ-ray was also measured in coincidence by the NaI(Tl) scintillation detector array called DALI2.

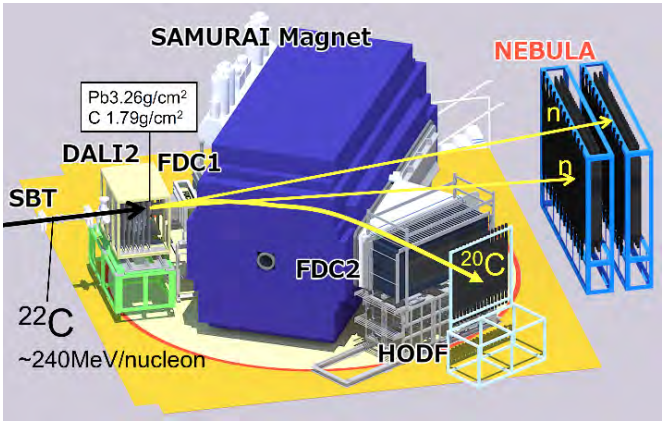

Fig. 4: The layout of SAMURAI, which consists of a large-gap superconducting dipole magnet, SBT (beam scintillator), BDC (beam MWDC, not shown here), FDC1, FDC2 (MWDCs for charged fragments), HODF (hodoscope for charged fragments), NEBULA (neutron detector array), and DALI2 (γ-ray detector array). As an example, the setup for the Coulomb breakup of ^{22}C is shown.

SAMURAI, commissioned in 2012, is a versatile spectrometer with much wider acceptance. In contrast to ZDS, it has a *single* superconducting dipole magnet with a large gap. In Fig. 4, the experimental setup for the Coulomb breakup of ^{22}C is shown schematically, where the incoming ^{22}C projectile, the outgoing ^{20}C fragment, and the two neutrons were measured in coincidence. One important aspect of SAMURAI is that it is ideally suited for kinematically complete measurements of the breakup reactions (e.g. Coulomb breakup). Other direct reactions, such as (p,n)-type charge exchange reactions [20] and (p,pn) [21] and (p,2p) quasi-free scattering in inverse kinematics, have also been studied. In this case, one can apply not only invariant mass spectroscopy that measures the momentum vectors for all the outgoing particles but also missing mass spectroscopy that measures the recoil particles from the target. In invariant mass spectroscopy, momenta of all the outgoing particles are measured to reconstruct the invariant mass of the intermediate excited state, while in missing mass spectroscopy coincidence measurements of the momenta of the beam and the recoil particles determine the excitation energy (mass) of the unmeasured residue. Such detailed spectroscopy experiments have become feasible owing to the large momentum and angular acceptance and rather good momentum resolutions (P/ΔP~1000) of SAMURAI [12]. The latter is important in identifying the charged particles. With SAMURAI, one can identify nuclei even in the mass region of ^{132}Sn, as was realized for the measurement of the ^{132}Sn(p,n) reaction [20].

^{22}C – New 2n halo nucleus and possible magic nucleus

^{22}C is the most neutron-rich bound carbon isotope at the neutron drip line, as shown in Fig.2. As the two neutron separation energy is very small (S_{2n} = −0.14(46) MeV) [22], and the conventional shell model predicts the dominance of the $2s_{1/2}$ configuration, ^{22}C has been a candidate for the prominent two-neutron halo nucleus. As the next s-wave two-neutron halo with $3s_{1/2}$ would be out of reach with the current and near-future RIB facilities, ^{22}C may be the last accessible s-wave 2n halo nucleus, probably for the next ten years. This nucleus is also important in terms of shell evolution as a candidate for the N=16 new magic nucleus as ^{24}O with N=16 is now an established doubly magic nucleus.

The first sign of the halo property of ^{22}C was obtained by Tanaka et al. [23], where the enhanced reaction cross section of ^{22}C with a proton target at 40 MeV/u was observed at RIPS (main RI-beam facility at RIKEN before the completion of RIBF). The rms radius of ^{22}C evaluated there was 5.4(9) fm. This value was then revised to 3.44(8) fm by the high-statistics reaction cross section measurement of ^{22}C on C target at 235 MeV/u at SAMURAI [24]. This rms radius is still significantly larger than ^{20}C, indicating the halo nature of ^{22}C. We should note that this reaction cross section was obtained as a by-product of the breakup experiment shown in Fig. 4, demonstrating the power of the large-acceptance spectrometer, SAMURAI.

At ZDS, the momentum distribution of ^{20}C following the breakup of ^{22}C on a carbon target was measured [25]. There, the narrow momentum distribution (about 73 MeV/c in FWHM) was observed as an indication of the 2n halo nucleus.

Coulomb breakup of ^{22}C was measured at SAMURAI with the setup shown in Fig. 4. Currently, the analysis of this experimental data is in progress, as well as that for the ^{21}C unbound states observed in the 1n removal channel in the reaction with the carbon target. The two-body constituent ^{21}C in the ^{22}C nucleus provides the key to understanding the shell structure of ^{22}C. Note that ^{22}C is a nucleus made of the three-body ^{20}C+n+n, called

Borromean, where any of the two-body constituents (^{20}C+n, n+n) are unbound and the three-body system (^{20}C+n+n) is bound. One of the crucial questions is whether the dineutron correlation exists in ^{22}C, and if so, how it appears. The dineutron correlation is considered to be the result of the mixed shell configuration of two neutrons in orbitals with different parities [3, 9]. As the shell configuration of ^{22}C should be very different from that of ^{11}Li, such investigations shed lights on the interplay between the dineutron correlation and the shell structure. We have Coulomb breakup data on ^{19}B as well, which is also under analysis. This may clarify the halo property of ^{19}B, and the possible mixture of s- and d-wave neutrons in this nucleus.

^{29,31}Ne, ^{37}Mg – Deformation driven p-wave halo

The island of inversion is a group of neutron-rich nuclei, which was originally addressed for Z=10–12 (Ne, Na, Mg), and N=20–22 in the nuclear chart [26], as schematically shown in Fig.2. The nuclei in the island are characterized by the loss of N=20 magicity and strong prolate deformation of the ground state. Such a property is attributed to the fact that the energy level of the 2p-2h intruder configuration lies lower than that of the normal configuration. How broad the island is extended in the nuclear chart is one of the key questions. Here I show ^{29}Ne [16], ^{37}Mg [19] are within the island of inversion, in addition to the firm confirmation of that for ^{31}Ne [17, 18]. The interplay between the halo phenomena and the shell evolution is expected to provide new insights in neutron-rich nuclei near the drip line. It is found that the deformation-driven p-wave halo is such a case.

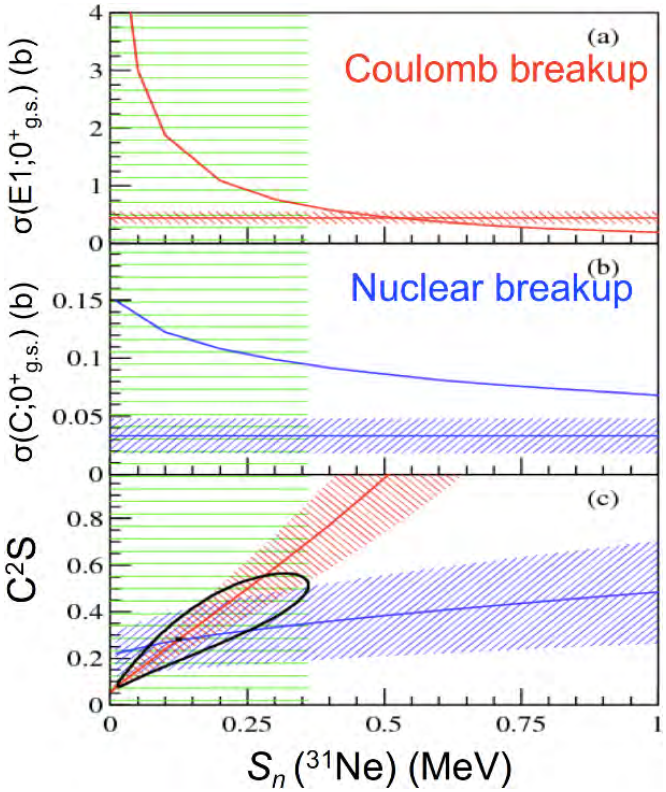

Fig. 5: (a) One-neutron removal cross sections of Coulomb breakup on Pb for ^{31}Ne decaying to the ^{30}Ne ground state, and (b) that on C. The cross sections are compared with theories for the configuration of a $2p_{3/2}$ neutron on the ^{30}Ne ground state with C^2S=1, which depends strongly on S_n. The Green area shows the S_n value from the direct mass measurement [22]. Comparison of each theory to the experimental data provides the allowed region in C^2S vs. S_n as shown in (c).

Before the RIBF was commissioned, experiments on ^{31}Ne and ^{37}Mg were almost impossible: Identification of these isotopes [27] was made only with the limited intensity of about five and one counts *per day* for ^{31}Ne and ^{37}Mg, respectively. RIBF changed this situation drastically, as ^{48}Ca beam at 345 MeV/u with strong intensity over 100 pμA, combined with the wide acceptance in-flight separator BigRIPS, offers intensities with 4-5 orders of magnitude larger. Even the first ^{31}Ne/^{37}Mg experiments at RIBF already provided about five counts per second (cps), and the recent record intensity of ^{31}Ne reached about 50 cps.

As one of the earlier experiments at RIBF, using the setup shown in Fig. 3, inclusive Coulomb and nuclear breakup of ^{31}Ne was investigated at about 230 MeV/u, where 'inclusive' means that the one-neutron removal cross section as well as the γ-ray from the ^{30}Ne core fragment were only measured without neutron coincidence. From this experiment, one can extract the one-neutron removal cross sections for decay directly to the ^{30}Ne ground state, both for C and Pb targets. The Coulomb breakup part of the one-neutron removal cross section on Pb was then deduced. One issue in extracting the structure information was the large uncertainty of the mass (S_n = −0.06±0.39 MeV [22]), since the one-neutron removal cross section in these reactions strongly depends on S_n.

The sensitivity to the halo amplitude is, on the other hand, quite distinctive between the nuclear- and Coulomb breakup, thereby providing a useful spectroscopic tool. Figure 5 compares the one neutron removal cross section for direct decay into ^{30}Ne for Coulomb breakup (a) and that for the breakup by the C target (b), with the theoretical calculations (Coulomb breakup: direct breakup model, Nuclear breakup: eikonal calculation).

The theoretical calculations are performed for the unit single-particle cross sections for the configuration of a p-wave valence neutron coupled to the ^{30}Ne ground state, and shown as a function of S_n, demonstrating the different sensitivities. We showed in Ref. [18] that only this configuration can explain the data. As shown in Fig.5(c), this comparison is then used to evaluate the spectroscopic factor $C^2S = 0.32^{+0.21}_{-0.17}$ for this configuration, and $S_n = 0.15^{+0.16}_{-0.10}$ MeV [18]. The value C^2S represents the overlap probability between the initial state (^{31}Ne) and the single-particle state (a neutron in $2p_{3/2}$) coupled to the core nucleus (^{30}Ne ground state). Currently, the S_n value obtained here is more accurate than the one from the direct mass measurement [22] and is included in the most recent standard mass evaluation, AME2016 [28].

This result shows that the spin-parity of ^{31}Ne is $3/2^-$, with significant contribution of the valence neutron in $2p_{3/2}$ orbital coupled to the ^{30}Ne ground state. Interestingly, such a ground state is out of the scope of the naïve shell model picture of $1f_{7/2}$ dominance and $7/2^-$ spin-parity for a N=21 nucleus. This result thus provides clear evidence that ^{31}Ne is in the island of inversion. Furthermore, such small separation energy and the significant p-wave (low-l) valence neutron favor the halo picture. The existence of the halo was independently confirmed by the enhancement of the reaction cross section measured at BigRIPS at RIBF [29].

This picture can be interpreted in terms of the Nilsson model (single-particle levels as a function of the quadrupole deformation parameter (β) calculated for a deformed mean-field potential) for a weakly bound neutron. For the 21st neutron, in the spherical limit (β=0), $1f_{7/2}$ and $2p_{3/2}$ levels are unbound and degenerate. Then the Jahn-Teller effect, deformation due to degeneracy of two configurations, occurs and the ground state becomes barely bound and strongly deformed. When the neutron separation energy is smaller, the p-wave neutron component is relatively more significant than the f-wave one since halo formation is favored to reduce the kinetic energy [30]. In this respect, the halo is formed due to the deformation with the enhanced p-wave component. Hence, ^{31}Ne provides the first confirmed case of *deformation-driven p-wave halo*. The large-scale shell model (shell model with large model space) shows large quadrupole transition probabilities (large B(E2) values) for the transition between the low-lying states, supporting the case for large deformation.

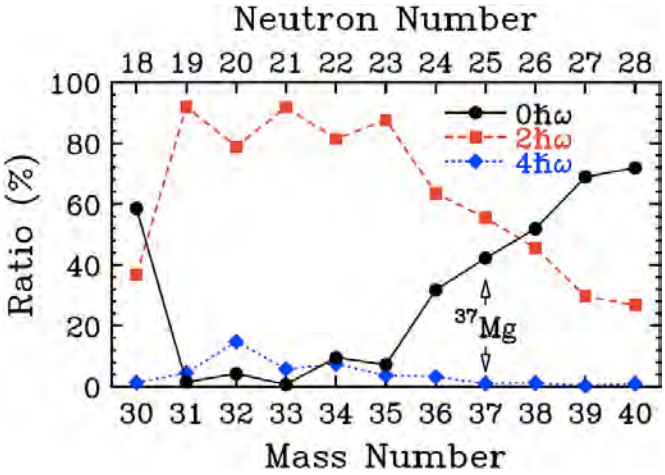

Fig. 6: Large-scale shell model calculation (SDPF-M) shows the occupancy of 2p-2h (red squares) is largest around N=19-23, and is becoming smaller towards N=28. At ^{37}Mg, this occupation is still significant and thus within the island of inversion. The figure is adopted from Ref. [19].

Using the same technique of combining inclusive Coulomb and nuclear breakup, we could find that the ground states of ^{37}Mg and ^{29}Ne are of negative parity, having the dominant configuration of $2p_{3/2}$, with strong deformation [16, 19]. Accordingly, we confirmed that ^{29}Ne and ^{37}Mg are also deformed-driven p-wave halo nuclei. Large rms radii for ^{29}Ne and ^{37}Mg indicated by the reaction cross section measurements confirmed their halo structure [29, 31]. ^{37}Mg represents currently the heaviest neutron halo nucleus confirmed. Figure 6 illustrates the occupations of normal 0p-0h (black dots) and intruder 2p-2h (red squares) configurations according to the neutron number for magnesium isotopes. A similar study is shown for ^{29}Ne in Ref.[16]. These studies show that ^{29}Ne is at the lower-mass edge of the island of inversion, and ^{37}Mg is near the higher-mass edge of the island. Recently, systematic studies of in-beam γ-ray spectroscopy observed the first 2^+ and 4^+ energies for the neutron-rich Mg isotopes [32, 33], and found that the deformation persists up to ^{40}Mg. This picture somewhat contradicts the calculation that the 2p-2h dominance is diminished towards ^{40}Mg in Fig.6. So not only the 2p-2h mechanism for N=20 but another mechanism such as the melting of the N=28 shell gap may play a role for the persistence of this strong deformation for a wider range of neutron-rich nuclei. Caurier, Nowacki, and Poves called this *big island of deformation* [34]. Note that even for ^{31}Ne and ^{37}Mg, the degeneracy of $2p_{3/2}$ and $1f_{7/2}$ (loss of N=28 gap) was observed, which indeed provided an important factor for p-wave halo formation.

Dineutron in Halo Nuclei?

Dineutron, as a spatially correlated pair, has not been directly observed so far. At RIBF, two approaches are in progress to search for dineutron. One method is Coulomb breakup of two-neutron halo nuclei, where the extracted low-lying E1 (electric dipole) strength as soft E1 excitation can be related to the geometrical two-neutron correlation as applied to ^{11}Li [10]. At SAMURAI, the Coulomb breakup experiments were performed for ^{19}B, ^{22}C, and the analysis is in progress.

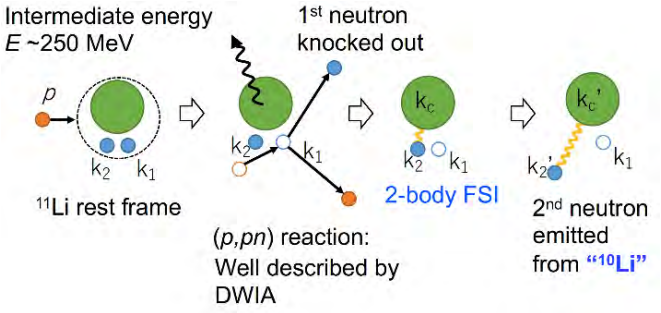

Fig. 7: Schematic concept of the quasi-free scattering of ^{11}Li(p,pn) is shown in the rest frame of ^{11}Li. The initial knockout process is used to determine the momentum of the first neutron inside ^{11}Li, while the momentum of the second neutron determines the residual core-n state.

The other approach is quasi-free (p,pn) scattering on two-neutron halo nuclei in inverse kinematics. Figure 7 shows a schematic concept of this method applied for ^{11}Li. The initial scattering of the proton with a neutron in the halo probes the momentum content of this neutron in the rest frame of the nucleus. Combined with the information of the second neutron relative to the ^{9}Li core, one can obtain the opening angle between the two neutrons. Accordingly, one can study the nn correlation as a function of the ^{10}Li state or the momentum of the neutron, which can provide a measure of how close to the surface the valence neutron is located. This method is based on theoretical considerations by Kikuchi [35]. At SAMURAI at RIBF, this method was applied to ^{11}Li, ^{14}Be, and ^{17}B [21, 36]. The preliminary analysis showed already some hint of dineutron in the surface of ^{11}Li [36].

It is noted that this method is also useful to observe the energy of the core-n system, which is crucial in understanding the three-body Borromean system of the two-neutron halo nuclei. Recently, using the ^{14}Be(p,pn) reaction in inverse kinematics, Corsi et al. clarified the shell structure of the unbound ^{13}Be nucleus, which had long been controversial [21].

Conclusions and Perspective

The key spectrometers, SAMURAI and ZDS, at RIBF have played significant roles in expanding the territory of halo nuclei in the neutron drip-line region of the nuclear chart. In this facility, the neutron halo structure was newly confirmed for ^{22}C, ^{29}Ne, ^{31}Ne, and ^{37}Mg. In particular, we note that the interplay between halo formation and shell evolution was found important in the neutron-drip line region of the island of inversion, as shown for ^{29,31}Ne and ^{37}Mg, where a deformation-driven p-wave halo is formed. Recently, the exclusive measurements of Coulomb and nuclear breakup of ^{31}Ne were made at SAMURAI, whose analysis is in progress. Here 'exclusive' means that both ^{30}Ne and the neutron from ^{31}Ne are measured in coincidence to reconstruct the ^{31}Ne excitation energy (invariant mass method). With this, one can extract the E1 strength as a function of the excitation energies, which would further pin-down the structure of ^{31}Ne. Such information is important to assess quantitatively the deformation and the shell property of deformation-driven p-wave halo nuclei. The quest for heavy halo nuclei and dineutron continues. At SAMURAI, we plan to build new types of neutron detector, one for the high-resolution high-granularity, HIME, and the other is NEBULA-PLUS to enhance the neutron detection efficiency in particular for multiple neutrons. With that, we expect to explore further heavier and more neutron-rich nuclei.

On the other hand, simpler experiments such as measurements of reaction cross sections and inclusive Coulomb and nuclear breakup are also important to obtain the first clue about a halo. Such experiments are useful in particular for very neutron-rich nuclei where the beam intensities are extremely weak (< one particle per second).

The possibility of neutron halo and its relation to the shell evolution in ^{27,29,31}F, ^{34}Ne, ^{34,37}Na ^{40}Mg will be interesting topics in the coming years as these are candidates for the next halo nuclei (see Fig.2). We should note that the observation of halo states in nuclei such as ^{31}Ne and ^{37}Mg, where the naive shell model picture does not allow the valence neutron to have low angular momentum, implies that halo nuclei may tend to appear all along the neutron drip line.

Recently, at TRIUMF in CANADA, low-energy RI beams were used to observe the low-lying resonance of ^{11}Li by inelastic scattering [37]. As soft E1 excitation in most halo nuclei showed a structure-less continuum [3, 4, 10],

it would be interesting to understand the characteristic features of such low-lying resonances.

The quest for nuclei beyond the neutron drip line is continuing. Recently, we have observed the *weakly unbound* nucleus ^{26}O [38], as well as heavy boron isotopes, ^{20,21}B [39], beyond the neutron drip line. These unbound resonances can be candidates for dineutron structure.

Combined with the intense RI-beams, with unique spectrometers such as SAMURAI and ZDS, and expecting new detectors such as HIME and NEBULA-PLUS, one would explore nuclei along the neutron drip line, thereby clarifying the halo properties, related exotic phenomena, and underlying many-body mechanism in the near future. This is also important for understanding the underlying mechanism of nucleo-synthesis in the universe such as the r-process, and the structure of neutron stars.

Acknowledgement: I would like to thank the accelerator staff at RIBF and the BigRIPS team for their excellent development and operation of the beams to realize the great success of experiments mentioned here. I also thank all the collaborators of the experiments using ZDS and SAMURAI. The present work was supported in part by JSPS KAKENHI Grant No. 22340053, No. 16H02179, and by MEXT KAKENHI Grants No. 24105005 and No. 18H05404. I thank Y. Kubota for providing figure (Fig.7).

References

[1] I. Tanihata et al., Phys. Rev. Lett. 55, 2676 (1985).
[2] I. Tanihata, H. Savajols, R. Kanungo, Prog. Part. Nucl. Phys. 68, 215 (2013).
[3] T. Nakamura, Y. Kondo, Clusters in Nuclei, Vol. 2, pp 67-119, (2012).
[4] T. Aumann, T. Nakamura, Phys. Scr. T152, 014012 (2013).
[5] T. Nakamura, H. Sakurai, H. Watanabe, Prog. Part. Nucl. Phys. 97, 53 (2017).
[6] D.S. Ahn et al., Phys. Rev. Lett. (2019), in press.
[7] A. B. Migdal, Sov. J. Nucl. Phys. 238 (1973).
[8] M. Matsuo, Phys. Rev. C 73, 044309 (2006).
[9] H. Sagawa, K. Hagino, Eur. Phys. J.A51, 102 (2015).
[10] T. Nakamura et al., Phys. Rev. Lett. 96, 252502 (2006).
[11] T. Kubo et al., Prog. Theo. Exp. Phys. 2012, 03C003(2012).
[12] T. Kobayashi et al., Nucl. Instr. Meth. B 317, 294 (2013).
[13] Y. Shimizu et al., Nucl. Instr. Meth. B 317, 739 (2013).
[14] H. Otsu, et al., Nucl. Instr. Meth. B 376, 175 (2016).
[15] T. Nakamura, Y. Kondo, Nucl. Instr. Meth. B 376, 156 (2016).
[16] N. Kobayashi et al., Phys. Rev. C 93, 014613 (2016).
[17] T. Nakamura, N. Kobayashi et al., Phys. Rev. Lett. 103, 262501 (2009).
[18] T. Nakamura, N. Kobayashi et al., Phys. Rev. Lett. 112, 142501 (2014).
[19] N. Kobayashi, et al., Phys. Rev. Lett. 112, 242501 (2014).
[20] J. Yasuda, et al., Phys. Rev. Lett. 121, 132501 (2018).
[21] A. Corsi, Y. Kubota et al., Phys. Lett. B 797, 134843 (2019).
[22] L. Gaudefroy et al., Phys. Rev. Lett. 109, 202503 (2012).
[23] K. Tanaka et al., Phys. Rev. Lett. 104, 062701 (2010).
[24] Y. Togano et al., Phys. Lett. B 761, 412 (2016).
[25] N. Kobayashi et al., Phys. Rev. C 86, 054604 (2012).
[26] E.K. Warburton, J.A. Becker, B.A. Brown, Phys. Rev. C 41, 1147 (1990).
[27] H. Sakurai et al., Phys. Rev. C 54. R2802 (1996).
[28] W.J. Huang, G. Audi, M. Wang, F.G. Kondev, S. Naimi, X.Xu, Chin. Phys. C41, 030002 (2017); M. Wang, G. Audi, F.G. Kondev, W.J. Huang, S. Naimi, X. Xu, Chin. Phys. C41, 030003 (2017).
[29] M. Takechi et al., Phys. Lett. B 707, 357 (2012).
[30] I. Hamamoto, Phys. Rev. C 81, 021304(R) (2010); I. Hamamoto, Phys. Rev. C 85, 064329 (2012).
[31] M. Takechi et al., Phys. Rev. C 90, 061305 (2014).
[32] P. Doornenbal, et al., Phys. Rev. Lett. 111, 212502 (2013).
[33] H.L. Crawford, et al., Phys. Rev. Lett. 122, 052501 (2019).
[34] E. Caurier, F. Nowacki, A. Poves, Phys. Rev. C 90, 014302 (2014).
[35] Y. Kikuch et al., Prog. Theor. Exp. Phys. 2016, 103D03 (2016).
[36] Y. Kubota, Doctoral Thesis, Univ. of Tokyo (2017).
[37] J. Tanaka et al., Phys. Lett. B 774, 268 (2017).
[38] Y. Kondo et al., Phys. Rev. Lett. 116, 102503 (2016).
[39] S. Leblond et al., Phys. Rev. Lett. 121, 262502 (2018).

Takashi Nakamura is Professor at the Department of Physics, School of Science, Tokyo Institute of Technology. He received D.Sci from the University of Tokyo in 1996. He worked at RIKEN, University of Tokyo, and Michigan State University before becoming an Associate Professor at Tokyo Institute of Technology in 2000. Since 2007, he has been is his current position. His research field is experimental nuclear physics.